Colloids and Surfaces B: Biointerfaces 133 (2015) 179–188

Contents lists available at ScienceDirect

Colloids and Surfaces B: Biointerfaces

journal homepage: www.elsevier.com/locate/colsurfb

A multi-layered vascular scaffold with symmetrical structure by bi-directional gradient electrospinning

Tong Wu[a], Chen Huang[b], Dawei Li[b], Anlin Yin[a], Wei Liu[c], Jing Wang[a], Jianfeng Chen[c], Hany EI-Hamshary[d,e], Salem S. Al-Deyab[d], Xiumei Mo[a,c,*]

[a] State Key Laboratory for Modification of Chemical Fibers and Polymer Materials, College of Chemistry, Chemical Engineering and Biotechnology, Donghua University, Shanghai 201620, China
[b] Engineering Research Center of Technical Textiles, Ministry of Education, College of Textiles, Donghua University, Shanghai 201620, China
[c] College of Material Science and Engineering, Donghua University, Shanghai 201620, China
[d] Department of Chemistry, College of Science, King Saud University, Riyadh 11451, Saudi Arabia
[e] Department of Chemistry, Faculty of Science, Tanta University, Tanta 31527, Egypt

ARTICLE INFO

Article history:
Received 21 January 2015
Received in revised form 2 May 2015
Accepted 29 May 2015
Available online 8 June 2015

Keywords:
Electrospinning
Multi-layered vascular scaffolds
P(LLA-CL)
Collagen
Chitosan
Tissue engineering

ABSTRACT

Multi-layered scaffolds are advantageous in vascular tissue engineering, in consideration of better combination of biomechanics, biocompatibility and biodegradability than the scaffolds with single structure. In this study, a bi-directional gradient electrospinning method was developed to fabricate poly(L-lactide-co-caprolactone) (P(LLA-CL)), collagen and chitosan based tubular scaffold with multi-layered symmetrical structure. The multi-layered composite scaffold showed improved mechanical property and biocompatibility, in comparison to the blended scaffold using the same proportion of raw materials. Endothelialization on the multi-layered scaffold was accelerated owing to the bioactive surface made of pure natural materials. hSMCs growth showed the similar results because of its better biocompatibility. Additionally, fibers morphology change, pH value balance and long term mechanical support results showed that the gradient structure effectively improved biodegradability.

1. Introduction

Clinically accredited vascular prostheses are increasingly desired as alternatives to autologous arterial or venous vascular substitutes because of the high mortality and disability caused by cardiovascular diseases. Although autograft is usually the most effective way, it has been often limited by the shortage of donors [1]. Besides, the acute thrombosis and subsequent occlusion often lead to the failure of the transplantation when commercialized Dacron or e-PTFE vascular grafts were used for small-diameter blood vessels [2]. In this regard, the unmet need drives the research into alternative tissue engineered vascular grafts for small diameter vessels [3]. Tissue engineered scaffolds aim at mimicking the natural extracellular matrix (ECM) both structurally and functionally to provide a suitable biophysiological microenvironment for tissue regeneration. As reported, ECM in native cardiovascular tissue plays a critical role for cells proliferation, motility and intercellular signaling, and the protein fibers along with other components in the ECM confer the structural integrity and mechanical support of blood vessels [4]. Therefore, choosing effective molding technologies and ECM-mimicking biomaterials is of great importance for designing bionic tissue engineered grafts.

Electrospinning is now a commonly utilized fabrication technique to prepare ultrafine fibers and fibrous scaffolds [5,6]. Electrospun scaffolds could offer more cues for cell growth because of the high surface area and porosity. Since the morphology and diameter of electrospun fibers depend on materials and processing parameters, through regulating these interrelated variables (*i.e.* spinneret design, electric field intensity, auxiliary electric/magnetic field, applied voltage, flow rate, collection distance, solution conductivity, and solution viscosity), fibers morphology can be well controlled [7].

A wide variety of natural and synthetic polymers have been electrospun for tissue engineered tubular scaffolds, including collagen, elastin, chitosan, polylactic acid (PLA), poly(ε-caprolactone) (PCL), poly(glycolic acid) (PGA), poly(L-lactide-co-caprolactone) (P(LLA-CL)), *etc.* [4,8–13]. Natural materials usually have better

* Corresponding author at: State Key Laboratory for Modification of Chemical Fibers and Polymer Materials, College of Chemistry, Chemical Engineering and Biotechnology, Donghua University, Shanghai 201620, China.
Tel.: +86 02167792653.
E-mail address: xmm@dhu.edu.cn (X. Mo).

http://dx.doi.org/10.1016/j.colsurfb.2015.05.048
0927-7765/

biocompatibility and lower thrombogenicity, while synthetic biomaterials could provide suitable mechanical support [14]. Collagen, as the primary structural component of natural ECM, could modulate the mechanical property of tissue engineered scaffolds and regulate cell adhesion, proliferation, *etc*. [4,15–18]. Chitosan is a biomimetic, amino cationic polysaccharide derived by deacetylation of chitin, which could emulate ECM glycosaminoglycan molecules and amplify the number of amine reaction sites and form an ionic complex with collagen that may result in enhanced stability [19–21]. Our previous efforts [8,22–24] suggested that collagen and chitosan based electrospun scaffolds could achieve optimal mechanical property and biocompatibility when the blending ratio was 4:1 (w/w). P(LLA-CL) was further mixed with collagen and chitosan blend as the reinforcement. When the ratio of P(LLA-CL)/collagen/chitosan was 75:20:5, the multicomponent nanofibrous scaffolds demonstrated good endothelial cell proliferation and mechanical support [13]. However, for blended scaffolds, direct contact of synthetic material with tissues could not be avoided, which often results in a relatively slow cell growth than natural scaffolds.

Recently, multi-layered scaffolds consist of both natural biomaterials and synthetic polymers have been designed and fabricated for vascular tissue engineering [14,25–29]. As reported, multilayered scaffolds could obtain diversified structure and have an advantage over homogeneous constructs, in view of the combination of mechanical properties, biodegradability, and biocompatibility [14,30–34]. However, some shortages restricted the development of multi-layered scaffolds like delamination or difficulty in molding three dimensional constructs with multiple components. To address the issue, we prepared a multi-layered vascular scaffold composed of natural biomaterials (collagen and chitosan) and synthetic polymer (P(LLA-CL)). P(LLA-CL) was set as the middle layer to provide mechanical support and extend degradation time. Collagen (COL) and chitosan (CS) (9:1, v:v) were set as the inner and outer layer to mimic the structure and components of natural ECM. Three transitional layers with gradient proportions of both components were respectively set between inner (or outer) layer and middle layer to regulate pore size and avoid delamination. The mechanical properties, cell-scaffold interaction and biodegradability of the scaffold were characterized *in vitro* to assess its potential in vascular tissue engineering.

2. Materials and experiments

2.1. Materials

P(LLA-CL) with 50% L-lactide was supplied by Gunze Ltd., Japan (molecular weight $\sim 3 \times 10^5$ Da). Collagen type I was purchased from Sichuan Mingrang Bio-Tech Co. Ltd., China (molecular weight 1×10^5 Da). Chitosan was bought from Sigma–Aldrich (viscosity 200,000 cps, medium molecular weight). 1,1,1,3,3,3-Hexafluoro-2-propanol (HFIP) was acquired from Fluorochem Ltd. (UK). 2,2,2-Trifluoroacetic acid (TFA) and a cross-linking agent of aqueous glutaraldehyde (GA) solution (25%) were procured from Sinopharm Chemical Reagent Co. Ltd., China. Porcine iliac artery endothelial cells (PIECs) and human smooth muscle cells (hSMCs) were obtained from the Institute of Biochemistry and Cell Biology (Chinese Academy of Sciences, China). All culture media and reagents were provided by Gibco Life Technologies Co. (USA) unless specified.

2.2. Scaffolds fabrication

P(LLA-CL) and collagen were separately dissolved in HFIP at the concentration of 8% (w/v) and chitosan was dissolved in the mixture of HFIP/TFA (9:1, v:v) at the concentration of 6% (w/v). The collagen and chitosan solutions were then blended with the ratio of 9:1 (v:v). A modified bi-directional gradient electrospinning (Fig. 1a) was employed to fabricate multi-layered vascular scaffolds with gradient symmetrical structure. “Gradient” in this study means that the proportions of natural or synthetic materials decreased or increased regularly from inner or outer layer to the middle layer. Specifically, the electrospinning solutions of P(LLA-CL) or COL/CS were filled into 10 mL plastic syringes with blunt-ended needles which were attached to two high voltage power supplies (BGG6-358, BMEI Co. Ltd., China), respectively. Two syringe pumps (789100C, Cole-Pamer, USA) were used in opposite directions. A stainless steel mandrel (4 mm diameter) with low rotating speed (300 rpm) was used to collect tubular scaffolds and a drum collector was used to prepare fibrous mats. A voltage of 14 kV was applied for P(LLA-CL) solution, and 20 kV was applied for COL/CS solution. To fabricate multi-layered vascular scaffold with gradient symmetrical structure, continuous bi-directional electrospinning was applied with the flow rates (mL/h) of COL/CS to P(LLA-CL) from inner layer to outer layer as follows: 0.8/0, 0.4/0.2, 0.2/0.4, 0.1/0.8, 0/1.6, 0.1/0.8, 0.2/0.4, 0.4/0.2, 0.8/0. For each flow rate, the electrospinning process was kept for 30 min.

As controls, pure P(LLA-CL), COL/CS (9:1, v:v) and P(LLA-CL)/COL/CS blended solution was electrospun respectively as described in Fig. 1b. In P(LLA-CL)/COL/CS blended solution, the volume ratio of P(LLA-CL) to COL/CS (9:1, v:v) was 22:15, in accordance with the proportion of multi-layered vascular scaffold. After preparing the scaffolds, samples with collagen and chitosan were cross-linked in a sealed desiccator with glutaraldehyde (GA) vapor (evaporating from 10 mL of 25% GA aqueous solution) at room temperature for 24 h, after which the samples were placed in the vacuum oven for 7 days.

2.3. Scaffolds characterization

Scanning electron microscopy (SEM) (JEOL JSM-5600, Japan) was used to observe the morphology of nanofibers and image analysis software (Image-J, National Institutes of Health, USA) was applied to analyze the average fiber diameter ($n = 100$) under lower magnification (1000×).

Confocal laser scanning microscopy (LSCM) (Carl Zeiss LSM 700, Germany) was utilized to observe the fiber distribution across the scaffolds. Firstly, the P(LLA-CL) solution was mixed with coomassie brilliant blue (CBB), while COL/CS solution was mixed with Rhodamine B. Because of the symmetrical structure, only half of the scaffold (from inner layer to middle layer) was prepared to observation. In this half part of the scaffold, the P(LLA-CL) fibers were stained with CBB and the COL/CS fibers were stained with Rhodamine B. Then *z*-axis scanning of LSCM was operated to observe fibers distribution.

2.4. Mechanical properties

Tensile mechanical property of all specimens (50 mm × 10 mm, $n = 6$) were characterized by a universal materials testing machine (H5K-S, Hounsfield, UK) at ambient temperature of 20 °C and humidity of 65%. A cross-head speed of 10 mm/min was used for all the specimens tested until breakage.

All samples were prepared for the same size (20 mm × 10 mm, ~0.06 mm in thickness, $n = 5$) and the suture retention strength was tested by micro material testing machine (MMT-250N, Shimadzu Co., Japan). Before testing, a loop of a 5–0 polyester suture (Shanghai Pudong Jinhuan Medical Products Co. Ltd., China) was placed 2 mm from the edge of one end of the sample, and the other end of the sample was clamped to one arm of the machine. Then the suture was clamped to the other arm and stretched at a constant rate of

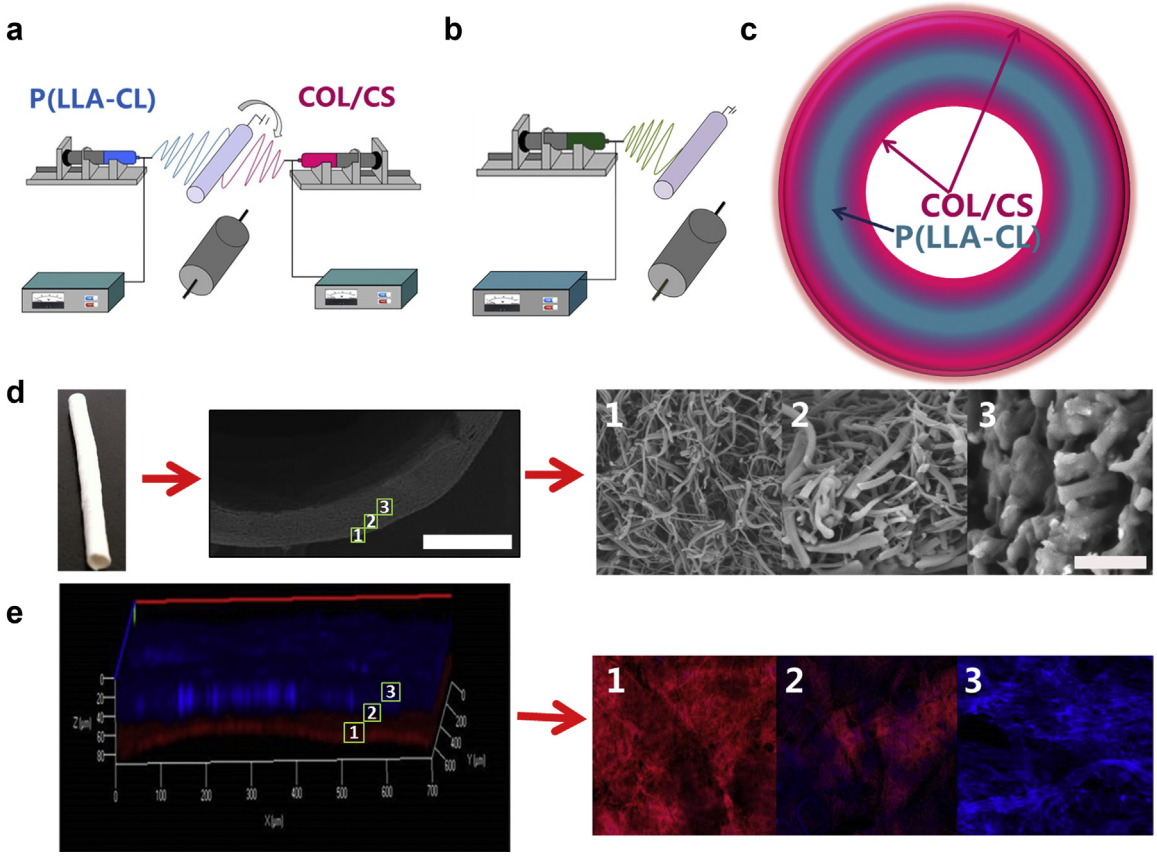

Fig. 1. (a) Schematic representation of the bi-directional gradient electrospinning setup; (b) schematic representation of the electrospinning setup for pure P(LLA-CL), COL/CS, and blended scaffolds; (c) schematic structure of the cross section of the multi-layered scaffold; (d) digital camera photograph of the tubular scaffold and scanning electron micrographs of the cross section; (e) confocal images showing fiber distribution of half thickness of the scaffold. 1: inner/outer layer, 2: transitional layer, 3: middle layer in d and e; scale bar in the left image = 500 μm and scale bar in the right image = 10 μm. (For interpretation of the references to color in text near the reference citation, the reader is referred to the web version of this article.)

120 mm/min until failure [35–37]. All samples were kept hydrated throughout the testing protocols, and the suture retention strength was defined as the maximum force obtained during the testing process.

Compliance testing was performed on the tubular scaffolds (3 mm of inner diameter and 5 cm of length, $n = 4$) using TM 1 Test Bench System (Bose Electro force, USA) in wet condition. The flow rate of the fluid was 100 mL/min and testing frequency was 1 Hz. Compliance under the pressure range of 80–120 mmHg was calculated as:

$$\%\text{Complliance} = \frac{(R_{P_2} - R_{P_1})}{R_{P_1}} \times \frac{10^4}{P_2 - P_1}$$

where R is the internal radius, P_1 is the lower internal pressure, and P_2 is the higher internal pressure [13].

2.5. Pore size

Pore size of all samples (30 mm × 30 mm, $n = 3$) were measured by a CFP-1100-AI capillary flow porometer (PMI Porous Materials Int.) before and after cross-linking.

2.6. Wettability

Surface wettability of different scaffolds was tested by measuring the contact angle of water droplets using a contact angle measurement instrument (OCA40, Dataphysics, Germany). 0.02 mL deionized water was used for each measurement and 6 different positions on each sample were averaged.

2.7. Cell viability and morphology

Porcine iliac artery endothelial cells (PIECs) and human smooth muscle cells (hSMCs) were respectively cultured in Dulbecco's modified Eagle's medium (DMEM) with 10% fetal bovine serum and 1% antibiotic–antimycotic in an atmosphere of 5% CO_2 and 37 °C, and the medium was replenished every two days. All electrospun samples were placed into 24-well plates individually and secured by stainless rings. Before seeding cells, all scaffolds and cover slips were sterilized by immersing in 75% ethanol for 2 h, washed 3 times with phosphate-buffered saline solution (PBS), and then washed once again with culture medium. For cell adhesion test, PIECs and hSMCs were both seeded with a density of 3.0×10^4 cells/well. For cell proliferation test, PIECs were seeded with a density of 1.0×10^4 cells/well, while hSMCs were seeded with a density of 3.0×10^4 cells/well.

Cells viability on different electrospun scaffolds was measured by methylthiazol tetrazolium (MTT) assay ($n = 3$ for each group). The cells and matrices were incubated with 5 mg/mL 3-[4,5-dimethyl-2-thiazolyl]-2,5-diphenyl-2H-tetrazolium bromide (MTT) for 4 h after 1, 2, 4, 8 h and 1, 3, 5, 7 days of cells seeding. Thereafter, the culture media were extracted and 500 μL dimethylsulfoxide (DMSO) were added for 20 min. When the crystal was sufficiently dissolved, aliquots were pipetted into the wells of a 96-well plate and measured for each well by an Enzyme-labeled

Instrument (Multiskan MK3, Thermo, USA) at an UV absorbance of 492 nm.

Cell adhesion and cell–fibers interaction was observed by SEM after 3 and 7 days of culturing. All samples in 24-well plates were rinsed twice with PBS and fixed in 2.5% GA solution at 4 °C for 4 h. Fixed samples were rinsed with PBS for three times and then dehydrated in gradient concentrations of ethanol (30%, 50%, 70%, 80%, 90%, 95% and 100%). After being dried in vacuum oven overnight, the samples were coated with gold sputter and observed under the SEM at a voltage of 10 kV.

Cell morphology and cell–cell interaction was observed by LSCM after 3 days of culture. All samples were rinsed twice with PBS and fixed in 4% paraformaldehyde for 1 h. After rising with PBS for three times, the samples were washed and permeabilized in 0.1% Triton X-100 (Sigma, USA) at room temperature for 5 min, and rinsed again with PBS for three times. Then 4′,6′-diamidino-2-phenylindole hydrochloride (DAPI, Invitrogen, USA) and rhodamine-conjugated phalloidin (Invitrogen, USA) were used to stain the nuclei and cytoskeletons of cells.

5×10^4 hSMCs were cultured on each electrospun scaffold for 7 days. Infiltration of hSMCs was analyzed with *Z*-stacked confocal microscopy. For each sample, 15 slices were pictured by LSCM, and subsequently imaging software ZEN 2008 (Carl Zeiss, Germany) was serviced to provide 3D images of the stained cells penetration into the scaffolds along *z*-axis.

2.8. Biodegradability

Different scaffolds were cut into rectangles (40 mm × 20 mm) for biodegradability test within the scheduled time (6 months) *in vitro*. The samples were placed in 15 mL of phosphate buffered solution (PBS, pH = 7.2 ± 0.1) in a water bath at 37 °C for predetermined periods of time. 2.0 mg sodium azide per 10 mL PBS was added to inhibit mold growth [38]. The PBS solution was replaced every month, and the degradation characterization of samples was measured. The degraded samples were washed completely with distilled water at room temperature, and then dried to constant weight in vacuum. The dried samples were weighted and the weight loss percentages were calculated from the dried weight obtained before and after degradation using gravimetrical method as the following relationships:

$$\text{Weight loss}\,(\%) = \frac{W_0 - W_d}{W_0} \times 100\%$$

where W_0 is the initial weight and W_d is the dry weight after degradation [38,39]. The pH value of PBS solution of different sample every month was measured by a digital pH meter. Each value was averaged from three specimens. The ultimate tensile stress and elongation of break of degraded sample was measured by a universal materials testing machine (H5K-S, Hounsfield, UK) every month until the sample could not be measured.

2.9. Statistics analysis

Statistics analysis was performed using origin 8.0 (Origin Lab Inc., USA). All the values were averaged at least in triplicate and expressed as means ± standard deviation (SD). Statistical differences were determined by the analysis of One-Way ANOVA and differences were considered statistically significant at $p < 0.05$.

3. Results and discussion

3.1. Morphology and structure

Before fabricating the multi-layered scaffolds, P(LLA-CL) and COL/CS with various flow rates were respectively electrospun.

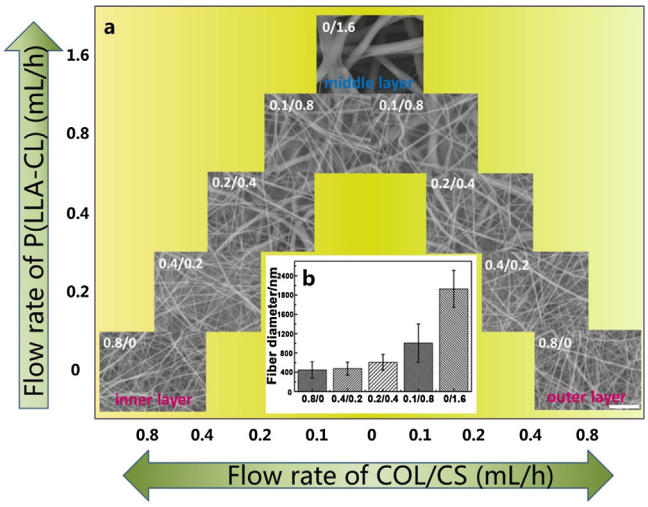

Fig. 2. (a) SEM images of different layers; (b) fiber diameter distribution of different layers; bar = 10 μm.

Through SEM observation, it is confirmed that both P(LLA-CL) and COL/CS were able to form continuous fibers under all the flow rates used in this study (Supporting information, Fig. S1). As shown in Fig. 1c, the inner and outer surfaces of the scaffold were both formed by collagen and chitosan, while the middle layer was formed by P(LLA-CL). By controlling the flow rates, the proportion of P(LLA-CL) decreased gradually from interior to surface, whereas proportion of COL/CS increased in gradients. Consequently, the inner and outer surfaces of the composite scaffold were composed of pure natural materials. Fig. 1d displays the micrographs of the multi-layered scaffold obtained by means of digital camera and SEM. The diameter range of nano-scale fibers in inner and outer layer was quite different from that of macro-scale fibers in the middle layer. Initially, the scaffold was fabricated by one layer of pure P(LLA-CL) and another layer of COL/CS, yet delamination of the layers often occurred due to the lack of affinity between natural and synthetic materials. The problem was solved by adding transitional layers between P(LLA-CL) and COL/CS layers. As the transitional layer contained both P(LLA-CL) and COL/CS fibers, no delamination was observed from the multilayered scaffolds. The difference in fibers morphology and diameter illustrated the components change in the multi-layered scaffold. Such change was further proved by confocal images in Fig. 1e. The red fibers were attributed to COL/CS component and the blue fibers were P(LLA-CL). The transitional layer displayed both blue and red fibers, indicating the mixture of P(LLA-CL) and COL/CS fibers.

Fig. 2a is SEM images of fiber morphology of each layer. It displayed the structural and morphological change of the fibers in different layers, which indicated the multi-layered symmetrical structure and components distribution of the composite scaffold. Fig. 2b is the quantification of the average fiber diameter of different electrospun scaffolds. The average values demonstrated the increase of the fiber diameter from inner (outer) layer to middle layer with the proportion of P(LLA-CL) increased. Statistical results suggested that the mean diameter of middle layer (2127 ± 381 nm) was significantly larger than that of the inner and outer layer (447 ± 169 nm) with the presence of COL/CS. It was mainly because the jets at the tip of needle were stretched due to the repulsive forces of static electricity during the electrospinning process. The positive charge carried by chitosan increased the solution conductivity and enhanced the stretch of jets.

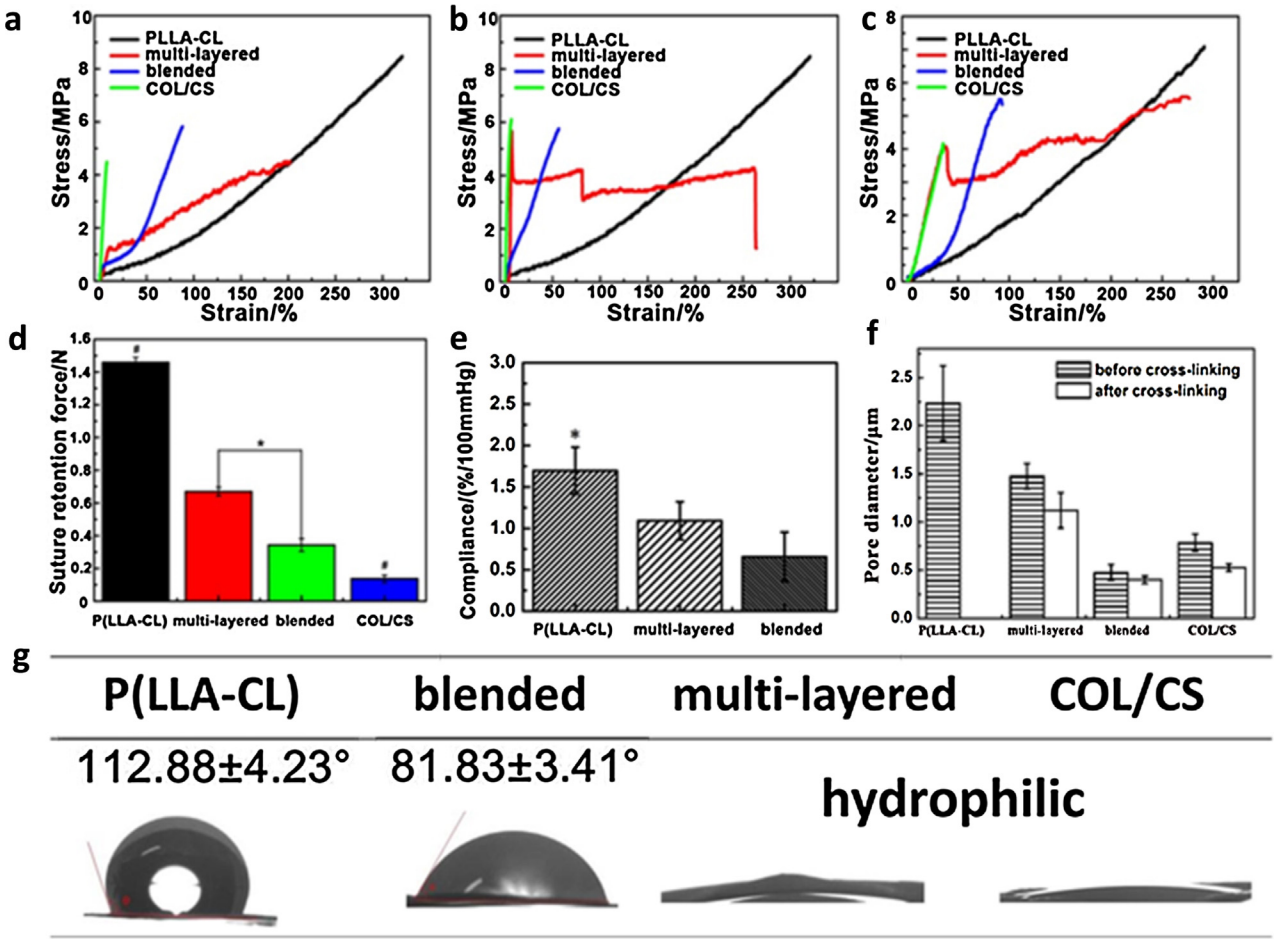

Fig. 3. Stress–strain curves of different electrospun scaffolds before cross-linking (a), after cross-linking in dry state (b) and in wet state (c); (d) suture retention force of the scaffolds with similar thickness; (e) compliance results of electrospun scaffolds in wet state; (f) pore diameter before and after cross-linking; (g) water contact angle of electrospun scaffolds.

3.2. Mechanical properties

Tensile results of all scaffolds are showed in Fig. 3 and Table 1. Fig. 3a shows the stress–strain curves of different electrospun scaffolds before cross-linking. Electrospun P(LLA-CL) scaffolds performed superior tensile stress and elongation, which was higher than COL/CS scaffolds. Stress and elongation of blended P(LLA-CL)/COL/CS scaffold and multi-layered scaffold were lower than P(LLA-CL) scaffold but higher than COL/CS scaffold (Table 1).

Fig. 3b shows the stress–strain curves of different scaffolds after GA cross-linking. Compared with the tensile curves before cross-linking, the stress values of pure COL/CS and blended scaffold respectively increased, but the strain values decreased. The stress value of multi-layered scaffold increased and the strain reduced (Table 1). It can be seen that the GA cross-linking process had a negative effect on the flexibility but a positive effect on mechanical stress of scaffolds with COL/CS. As shown by the curve, the breakage style of multi-layered scaffold experienced several stages during stretch. Firstly, it tended to be stiffer with a higher initial modulus due to the cross-linked COL/CS surface. After a rapid breakage and sharp yield, the stretch of the multilayers leaned toward stable except for a moderate drop until the final fracture. This curve had a reasonable tendency because P(LLA-CL) fibers and COL/CS fibers of the multi-layered scaffold were integrated by the symmetrically

Table 1
Tensile property of all scaffolds.

Specimen		Average tensile strength (MPa)	Average elongation at break (%)
P(LLA-CL)	Dry	8.54 ± 0.71	314.33 ± 7.77
	Wet	7.22 ± 0.37	290.01 ± 9.25
Blended	Before cross-linking (dry)	5.78 ± 0.56	88.33 ± 8.50
	After cross-linking (dry)	5.90 ± 3.30	56.8 ± 3.82
	After cross-linking (wet)	5.50 ± 0.49	93.33 ± 5.51
Multi-layered	Before cross-linking (dry)	4.57 ± 0.31	203.15 ± 4.64
	After cross-linking (dry)	5.85 ± 0.52	264.77 ± 6.60
	After cross-linking (wet)	5.76 ± 0.60	276.22 ± 7.01
COL/CS	Before cross-linking (dry)	4.48 ± 0.41	7.99 ± 0.67
	After cross-linking (dry)	6.10 ± 0.30	6.85 ± 0.68
	After cross-linking (wet)	4.40 ± 0.52	38.95 ± 8.59

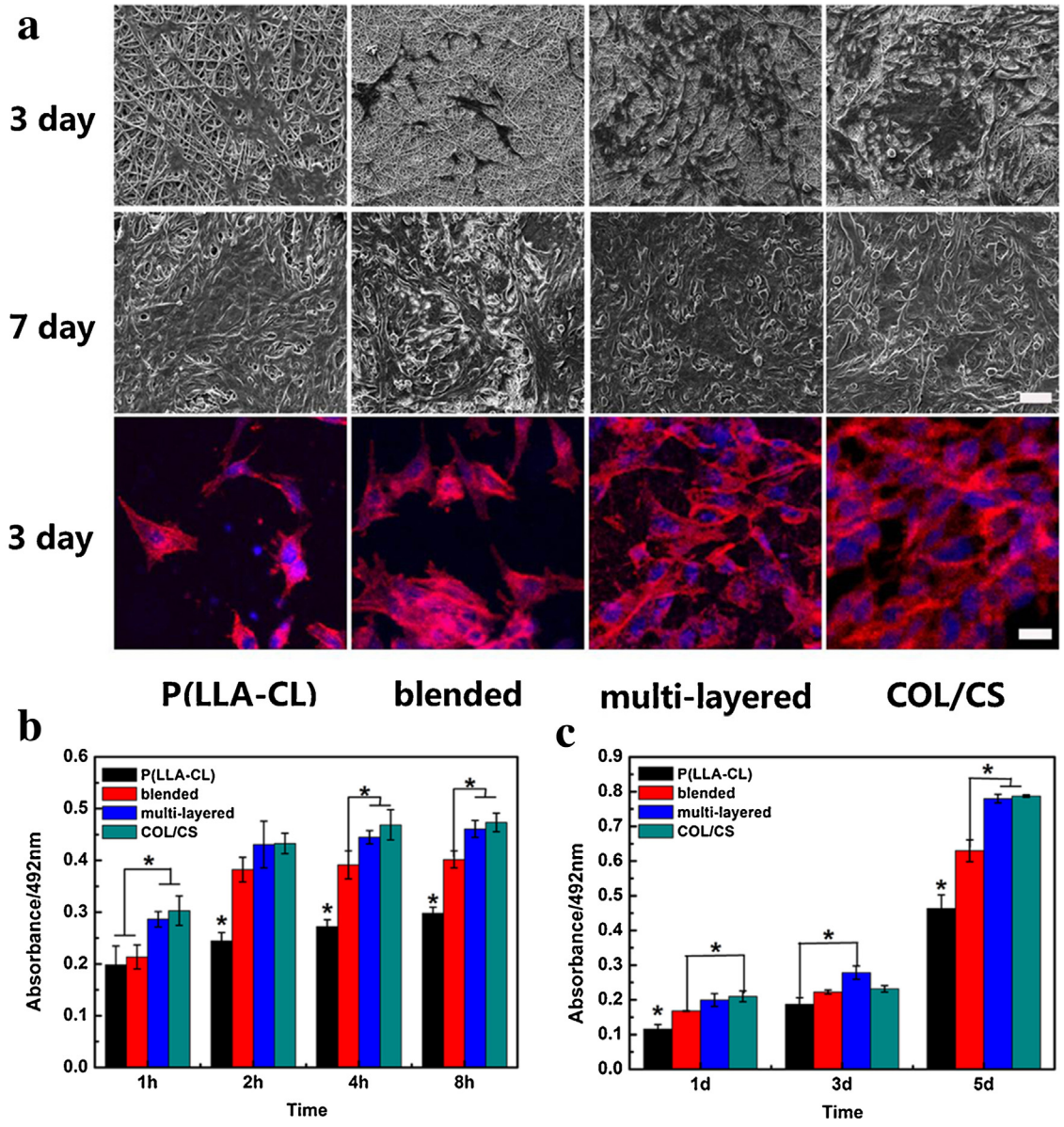

Fig. 4. Scanning electron micrographs of PIECs on different scaffolds after culturing for 3 and 7 days, and confocal images of PIECs on different scaffolds after culturing for 3 days (a); adhesion and proliferation of PIECs after culturing in 8 h (b) and 5 days (c); bar = 25 μm.

gradient electrospinning method. As expected, the tensile behavior of multi-layered scaffold performed the characteristic of outer layer (COL/CS) at first. Following, several outer transitional layers shed first, and then other internal transitional layers broke gradually. In this process, the tension changed slightly. Finally, the middle layer gradually exposed with stable stress and optimal tensile elongation, exhibiting a highly similar tensile behavior to P(LLA-CL) scaffolds.

Fig. 3c shows the stress–strain curves of different scaffolds in wet state. P(LLA-CL) scaffold was still of the strongest mechanical property, while the COL/CS scaffold stayed the weakest. The maximal tensile strength of blended and multi-layered scaffold remained the same as a consequence of the identical composition and proportion, but the elongation at break of multi-layered scaffold was much larger than that of the blended one (Table 1). In the fabrication of vascular scaffolds, better mechanical properties were of crucial importance to provide sufficient support, especially in consideration of degradation and strength loss in wet state. Since most of the materials used in tissue engineering were required to be biodegradable, raw materials should possess higher mechanical strength and elongation [40–42]. As reported, the adventitial layer of the coronary arteries had an ultimate tensile stress of ~1.4 ± 0.6 MPa, and the ultimate strain of human coronary artery was 45–99% [13,33]. Also, the tensile stress of a natural infrarenal aorta was 4.4 ± 0.9 MPa [35]. The results inferred that the tensile property of the multi-layered scaffold was able to match that of a native artery, even considering biodegradation.

Suture retention forces are given in Fig. 3d. Pure P(LLA-CL) scaffold showed the highest suture force (1.46 ± 0.03 N) and COL/CS was the lowest (0.14 ± 0.02 N), and both of those had significant differences ($p < 0.05$) with the other three groups. By mixing P(LLA-CL) and COL/CS components, the maximum suture retention forces of blended (0.34 ± 0.04 N) and multi-layered scaffold (0.67 ± 0.03 N) were both larger than those of COL/CS scaffold. As reported, strength of scaffolds relied largely on the strength of single fiber [22]. For blended scaffolds, P(LLA-CL) and COL/CS was mixed before electrospinning, whereas the bi-directional gradient electrospinning blended P(LLA-CL) and COL/CS fibers during the electrospinning process. Thus, the abundant P(LLA-CL) fibers in

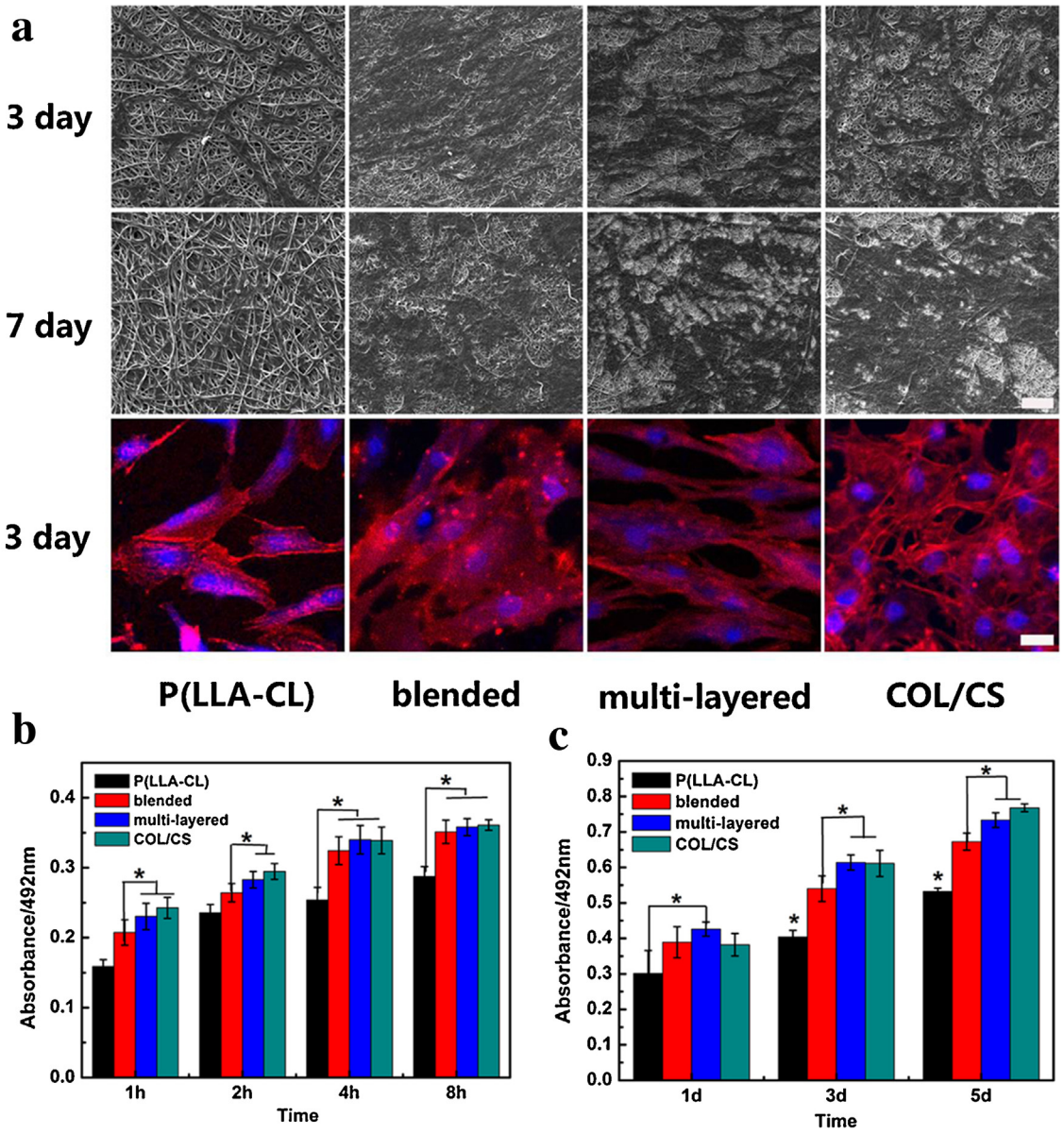

Fig. 5. (a) Scanning electron micrographs of hSMCs on different scaffolds after culturing for 3 and 7 days, and confocal images of hSMCs on different scaffolds after culturing for 3 days; adhesion and proliferation of hSMCs after culturing in 8 h (b) and 5 days (c); bar = 25 μm.

transitional and middle layer of the multi-layered scaffolds could play a crucial role to provide sufficient mechanical support for the joints between suture lines and scaffolds.

Compliance results of different scaffolds were showed in Fig. 3e. Pure P(LLA-CL) possessed an average of 1.70%/100 mmHg, which was significantly higher ($p < 0.05$) than other scaffolds. Owning to the high elasticity of P(LLA-CL) fibers from middle layers, the multi-layered scaffolds had better compliance than the blended one. The compliance value was similar to that of the saphenous vein (0.7–1.5%/100 mmHg) [13].

3.3. Pore size

Fig. 3f shows the average pore diameter of different groups before and after GA cross-linking. The pore size of the multi-layered composite scaffolds decreased from 1.48 ± 0.13 μm to 1.12 ± 0.18 μm after GA cross-linking. This was due to the distortion of COL/CS components on surface, as they formed a denser structure after cross-linkage. The average pore size of pure P(LLA-CL) scaffold was the largest among the four groups with the value of 2.24 ± 0.39 μm, owing to the largest diameter of P(LLA-CL) fibers. The average pore size values of the multi-layered scaffold before and after cross-linking were larger than those of the blended scaffold, owing to the presence of single P(LLA-CL) fibers in the middle layer and transitional layers in the multi-layered scaffold.

3.4. Wettability

Surface wettability of biomaterials greatly affected cell adhesion, proliferation and migration. In Fig. 3g, synthetic P(LLA-CL) scaffolds were hydrophobic with a water contact angle larger than 90° and natural COL/CS scaffolds were hydrophilic. With the addition of collagen and chitosan, hydrophilicity of blended scaffolds was improved (Fig. 3g). The wetting process of multi-layered scaffolds was nearly the same as COL/CS scaffolds, as the surface of the multi-layered scaffold did not consist of any synthetic polymer.

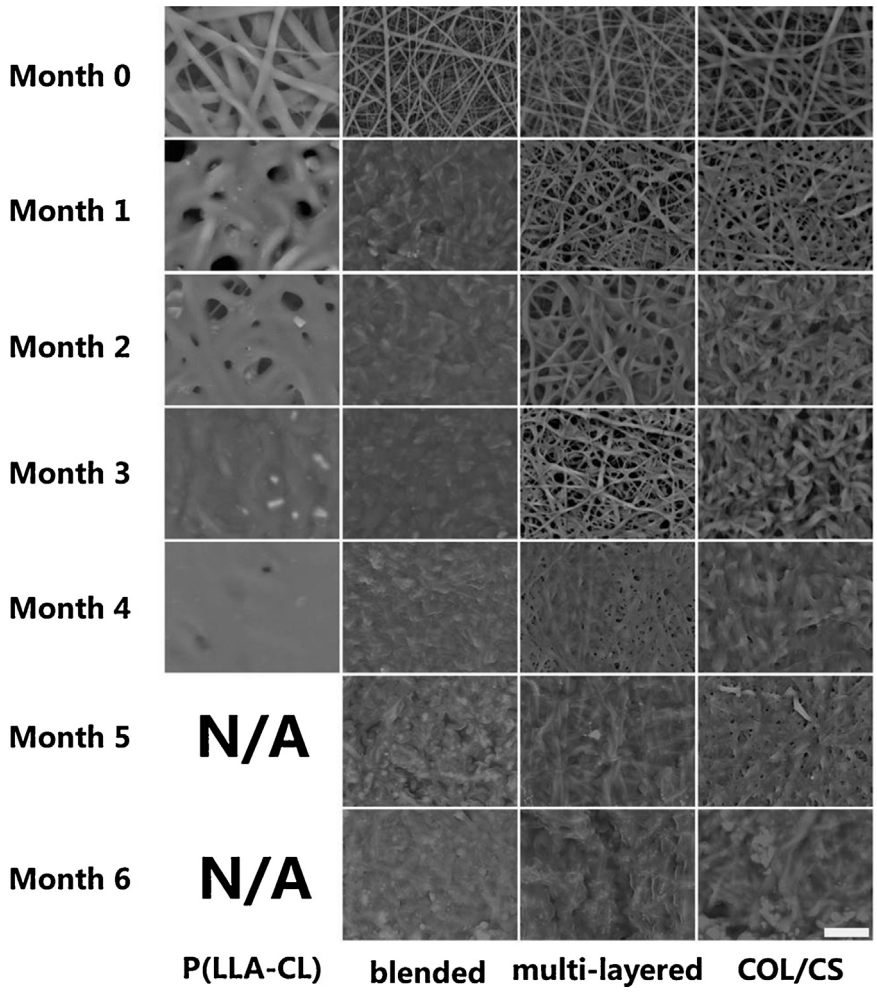

Fig. 6. Scanning electron micrographs of different scaffolds after biodegradation for different periods; bar = 10 μm.

3.5. Cell viability and morphology

Fig. 4a shows SEM and confocal images of PIECs after culturing for 3 and 7 days. PIECs were found to spread more easily on multi-layered and COL/CS scaffolds. At day 7, the surface of multi-layered scaffolds was covered by successive and structured endothelial cell monolayer, while cell number was much lower on blended and P(LLA-CL) scaffolds. Confocal images confirmed the same trend as PIECs tended to spread better on pure natural surface and had better cell junction than on synthetic and blended surfaces. It was because the fibers on multi-layered and pure COL/CS surfaces could provide larger specific surface for cell spreading than the fibers on P(LLA-CL) scaffolds. Also, the natural surfaces exposed more bioactive functional groups and thus improved the interaction between scaffolds and cells. Fig. 4b shows PIECs adhesion after seeding on different scaffolds in 8 h, and Fig. 4c shows PIECs proliferation viability after seeding on different scaffolds in 5 days. Adhesion values of COL/CS and multi-layered scaffolds were significantly higher than those of other groups, regardless of culture time. The results indicated that COL/CS surface improved the biocompatibility of multi-layered scaffolds. After 1 day of culture, cell proliferation showed a similar trend. The results suggested that, in comparison to the blended scaffolds, the multi-layered composite scaffolds having a pure natural materials based surface could effectively enhance the adhesion and proliferation of PIECs.

hSMCs growth behaviors are exhibited in Fig. 5. hSMCs grew better on the scaffolds with natural COL/CS components than on the P(LLA-CL) scaffold. Also, hSMCs on multi-layered scaffolds appeared obviously stretched cell structure and less cell aggregation compared to the blended counterparts, mainly because of its pure natural surface and the larger growth space inside the multi-layered construction. Statistical results in Fig. 5b and c suggested that electrospun scaffolds with pure natural surfaces had better cell viability than P(LLA-CL) and blended scaffolds. Three-dimensional growth of hSMCs on multi-layered and blended scaffold was observed by *Z*-stacked confocal microscopy. The images suggested that, in comparison to blended scaffolds, the larger space inside the multi-layered construction effectively promoted cells penetration (Supporting information, Fig. S2).

3.6. *Biodegradability* in vitro

SEM images of different electrospun scaffolds before and during the degradation process are shown in Fig. 6. Generally, the degradation of P(LLA-CL) scaffolds experienced a "swelling-bonding-melting" process. P(LLA-CL) fibers began to swell and bond since the first month. After 3 months, fibers were melted totally and no obvious fibers structure could be seen through SEM observation. This was mainly caused by the decrease of the molecular weight of P(LLA-CL) [38]. As a rubbery state polymer, molecular chains of P(LLA-CL) became mobilized when its glass transition temperature was near or below the experimental temperature, and the fibers tended to "melt" together to reduce the surface tension [40,43,44]. Consequently, P(LLA-CL) scaffold became viscous and

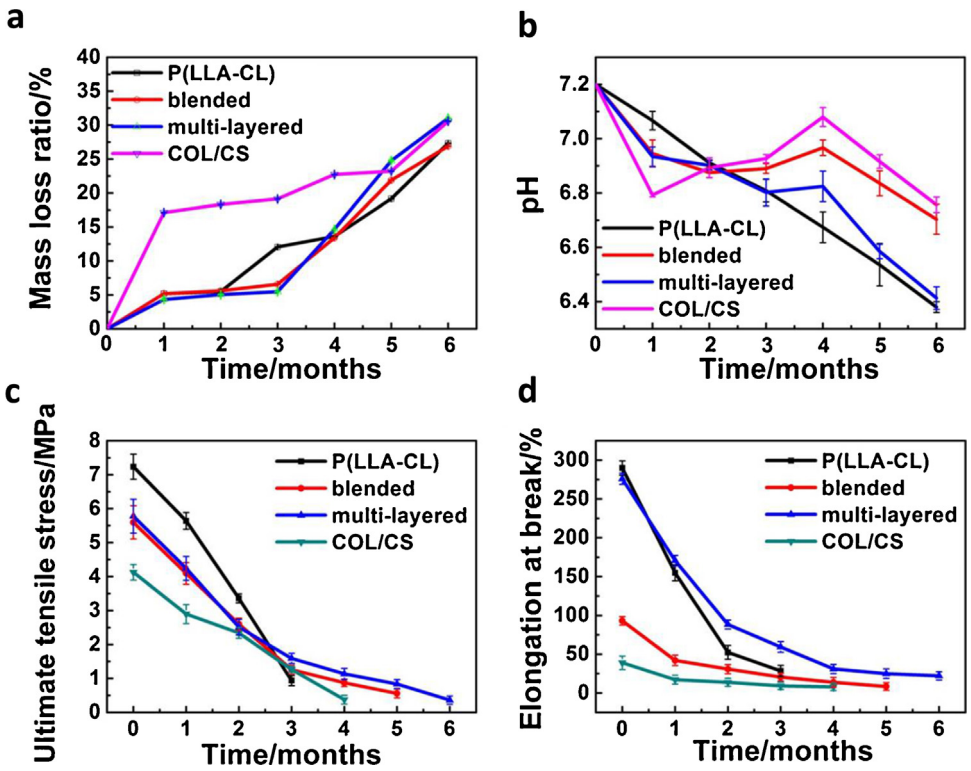

Fig. 7. Mass loss percentage (a), pH value change (b), ultimate tensile stress (c), elongation at break (d) of different scaffolds after biodegradation for different periods.

adhesive on a macro level. By contrast, no obvious morphological change was found in natural COL/CS nanofibrous scaffolds till month 2. After month 3, COL/CS nanofibers distorted seriously and started to melt and break at month 4. However, for blended and multi-layered scaffolds consisted of the same components proportion, the morphology change of nanofibers distinguished totally. Fibers in blended scaffolds began to swell and melt from the first month, which was similar to P(LLA-CL) scaffolds. After month 2, all fibers on the surfaces were melted together. This was mainly because different components were blended in one single fiber and P(LLA-CL) accounted for the largest amount. Different from blended scaffolds, degradation of the multi-layered scaffolds was closer to COL/CS scaffolds. After degradation for 1 month, the surface was partly dissolved, but the integral fiber structure was well remained. From month 2, the surface fibers began to adhere and break, subsequently a large area of fibers were bonded and melted gradually with no fibers could be seen after 5 months.

In multi-layered scaffolds, the integral structure could be better remained at the early stage till month 3. A reasonable explanation was that the scaffolds were composed of two kinds of fibers: the symmetrical hydrophilic COL/CS surfaces and inner hydrophobic P(LLA-CL) fibers. The same natural surfaces made the degradation process of multi-layered scaffolds similar to natural COL/CS scaffolds in the early periods. This proved that the symmetrical structure of multi-layered scaffolds contributed to maintain fibers morphology and extended the duration of degradation than blended and P(LLA-CL) scaffolds. It is believed that the degradation time can be further tailored by using the same electrospinning method with different proportions of COL, CS and P(LLA-CL).

Fig. 7a describes the mass loss ratio of different groups in the degradation periods. Despite of the severe morphological change, the mass loss of pure P(LLA-CL) rose gradually to 27.3% till month 6, mainly because that the degradation products of P(LLA-CL) were insoluble in PBS. However, the mass loss of COL/CS scaffolds changed dramatically since month 1, due to the dissolution of some uncross-linked fibers in the degradation medium. Also, the hydrolysis products of natural protein and polysaccharide were water soluble, leading to a quick mass loss. Compared with natural polymer, longer periods were taken for the mass loss in blended scaffold and multi-layered scaffold, mainly because different components were mixed in one fiber in blended scaffold and two kinds of fibers were composited in multi-layered scaffolds. Finally with the fibers degradation, the mass loss ratios increased from month 3 and finally reached almost to 30%.

Fig. 7b shows the pH value change of degradation medium during the degradation process. As the degradation medium was changed every month, the pH value curves in the graph indicated the change in each degradation month. For pure P(LLA-CL) scaffold, the pH value kept decreasing during the degradation periods, while that of COL/CS scaffold only fluctuated in a near-neutral range. Due to the mixture of P(LLA-CL) and COL/CS in blended scaffold and the wrapping of COL/CS surfaces for the interior P(LLA-CL) in multi-layered scaffold, the degradation of P(LLA-CL) component was postponed.

The tensile stress and elongation of the electrospun scaffolds in different degradation time are shown in Fig. 7c and d. As illustrated by Fig. 7c, P(LLA-CL) scaffold had the highest strength and the value of COL/CS scaffold remained the lowest among all the groups after degradation for 1 and 2 months. However, with the degradation of P(LLA-CL) fibers, the maximal tensile stress decreased at month 3, and after that P(LLA-CL) scaffolds started to be viscous and could not be measured because of the P(LLA-CL) molecular weight decrease [38]. As a result, the mechanical property of P(LLA-CL) fibers suffered a great loss. Conversely, the maximal tensile stress values of blended and multi-layered scaffold were both gradually declined, and the strength of multi-layered scaffold was able to maintain around 2 MPa after 3 months in the biodegradation environment, which was larger than those of the other three groups.

In Fig. 7d, the elongation values of P(LLA-CL) and multi-layered scaffold were the highest two groups, because of the better

elasticity of P(LLA-CL) fibers. Although the initial flexibility of P(LLA-CL) scaffold was slightly better than multi-layered scaffold, the elongation of multi-layered scaffold retained the best from month 1 to month 6. Because P(LLA-CL) fibers were wrapped by COL/CS fibers, the inner P(LLA-CL) fibers were protected from being degraded rapidly. Finally the multi-layered scaffold could still keep an elongation of ~50% after 6 months of degradation. The degradation results suggested that the multi-layered symmetrical structure could better preserve the mechanical performance of the scaffold.

4. Conclusions

In this study, a novel vascular tissue-engineered scaffold with symmetrical gradient structure was successfully developed by using the bi-directional electrospinning method. The symmetrical structure made the multi-layered scaffold an optimal composition between synthetic and natural biomaterials. The multi-layered scaffold exhibited a combination of excellent mechanical property and high biocompatibility. It also provided longer mechanical support during the biodegradation process, making the scaffold an ideal candidate for vascular tissue engineering.

Acknowledgements

This research was supported by National Nature Science Foundation of China (31470941, 31271035, 51403033), Science and Technology Commission of Shanghai Municipality (11nm0506200), Ph.D. Programs Foundation of Ministry of Education of China (20130075110005) and light of textile project (J201404) and the Fundamental Research Funds for the Central Universities. The authors would like to extend their sincere appreciation to the Deanship of Scientific Research at King Saud University for its funding of this research through the research group project No. RGP-201.

Appendix A. Supplementary data

Supplementary data associated with this article can be found, in the online version, at http://dx.doi.org/10.1016/j.colsurfb.2015.05.048

References

[1] Y. Yao, J. Wang, Y. Cui, R. Xu, Z. Wang, J. Zhang, K. Wang, Y. Li, Q. Zhao, D. Kong, Acta Biomater. 10 (2014) 2739–2749.
[2] Z. Wang, Y. Cui, J. Wang, X. Yang, Y. Wu, K. Wang, X. Gao, D. Li, Y. Li, X.-L. Zheng, Y. Zhu, D. Kong, Q. Zhao, Biomaterials 35 (2014) 5700–5710.
[3] C. Saitow, D.L. Kaplan, J.J. Castellot Jr., Matrix Biol. 30 (2011) 346–355.
[4] X. Zhang, V. Thomas, Y. Xu, S.L. Bellis, Y.K. Vohra, Biomaterials 31 (2010) 4376–4381.
[5] H. Zhang, X. Jia, F. Han, J. Zhao, Y. Zhao, Y. Fan, X. Yuan, Biomaterials 34 (2013) 2202–2212.
[6] C. Vaquette, J.J. Cooper-White, Acta Biomater. 7 (2011) 2544–2557.
[7] B. Sun, Y.Z. Long, H.D. Zhang, M.M. Li, J.L. Duvail, X.Y. Jiang, H.L. Yin, Prog. Polym. Sci. 39 (2014) 862–890.
[8] Z.G. Chen, P.W. Wang, B. Wei, X.M. Mo, F.Z. Cui, Acta Biomater. 6 (2010) 372–382.
[9] T.H. Nguyen, A.R. Padalhin, H.S. Seo, B.T. Lee, J. Biomater. Sci.: Polym. Ed. 24 (2013) 1692–1706.
[10] E.S. Fioretta, J.O. Fledderus, E.A. Burakowska-Meise, F.P. Baaijens, M.C. Verhaar, C.V. Bouten, Macromol. Biosci. 12 (2012) 577–590.
[11] F. Du, H. Wang, W. Zhao, D. Li, D. Kong, J. Yang, Y. Zhang, Biomaterials 33 (2012) 762–770.
[12] S. Chung, N.P. Ingle, G.A. Montero, S.H. Kim, M.W. King, Acta Biomater. 6 (2010) 1958–1967.
[13] A. Yin, K. Zhang, M.J. McClure, C. Huang, J. Wu, J. Fang, X. Mo, G.L. Bowlin, S.S. Al-Deyab, M. El-Newehy, J. Biomed. Mater. Res. A 101 (2013) 1292–1301.
[14] S. Liu, C. Dong, G. Lu, Q. Lu, Z. Li, D.L. Kaplan, H. Zhu, Acta Biomater. 9 (2013) 8991–9003.
[15] J.A. Matthews, G.E. Wnek, D.G. Simpson, G.L. Bowlin, Biomacromolecules 3 (2002) 232–238.
[16] P. Buijtenhuijs, L. Buttafoco, A.A. Poot, W.F. Daamen, T.H. Van Kuppevelt, P.J. Dijkstra, R.A.I. De Vos, L.M.T. Sterk, B.R.H. Geelkerken, J. Feijen, I. Vermes, Biotechnol. Appl. Biochem. 39 (2004) 141–149.
[17] B.-S. Kim, D.J. Mooney, J. Biomech. Eng. 122 (2000) 210–215.
[18] M. Li, M.J. Mondrinos, M.R. Gandhi, F.K. Ko, A.S. Weiss, P.I. Lelkes, Biomaterials 26 (2005) 5999–6008.
[19] M. Rafat, F. Li, P. Fagerholm, N.S. Lagali, M.A. Watsky, R. Munger, T. Matsuura, M. Griffith, Biomaterials 29 (2008) 3960–3972.
[20] A. Sionkowska, Biomaterials 25 (2004) 795–801.
[21] J. Berger, M. Reist, J.M. Mayer, O. Felt, N.A. Peppas, R. Gurny, Eur. J. Pharm. Biopharm. 57 (2004) 19–34.
[22] Z. Chen, X. Mo, C. He, H. Wang, Carbohydr. Polym. 72 (2008) 410–418.
[23] Z. Chen, X. Mo, F. Qing, Mater. Lett. 61 (2007) 3490–3494.
[24] Z. Chen, B. Wei, X. Mo, C.T. Lim, S. Ramakrishna, F. Cui, Mater. Sci. Eng. C 29 (2009) 2428–2435.
[25] B. Marelli, M. Achilli, A. Alessandrino, G. Freddi, M.C. Tanzi, S. Farè, D. Mantovani, Macromol. Biosci. 12 (2012) 1566–1574.
[26] F. Han, X. Jia, D. Dai, X. Yang, J. Zhao, Y. Zhao, Y. Fan, X. Yuan, Biomaterials 34 (2013) 7302–7313.
[27] Y.M. Ju, J.S. Choi, A. Atala, J.J. Yoo, S.J. Lee, Biomaterials 31 (2010) 4313–4321.
[28] M.J. McClure, S.A. Sell, D.G. Simpson, B.H. Walpoth, G.L. Bowlin, Acta Biomater. 6 (2010) 2422–2433.
[29] M.J. McClure, D.G. Simpson, G.L. Bowlin, J. Mech. Behav. Biomed. Mater. 10 (2012) 48–61.
[30] L. Soletti, Y. Hong, J. Guan, J.J. Stankus, M.S. El-Kurdi, W.R. Wagner, D.A. Vorp, Acta Biomater. 6 (2010) 110–122.
[31] S. de Valence, J.C. Tille, J.P. Giliberto, W. Mrowczynski, R. Gurny, B.H. Walpoth, M. Moller, Acta Biomater. 8 (2012) 3914–3920.
[32] M. Sato, Y. Nakazawa, R. Takahashi, K. Tanaka, M. Sata, D. Aytemiz, T. Asakura, Mater. Lett. 64 (2010) 1786–1788.
[33] S.G. Wise, M.J. Byrom, A. Waterhouse, P.G. Bannon, A.S. Weiss, M.K. Ng, Acta Biomater. 7 (2011) 295–303.
[34] S. Shinohara, T. Kihara, S. Sakai, M. Matsusaki, M. Akashi, M. Taya, J. Miyake, J. Biosci. Bioeng. 116 (2013) 231–234.
[35] H. Bergmeister, C. Schreiber, C. Grasl, I. Walter, R. Plasenzotti, M. Stoiber, D. Bernhard, H. Schima, Acta Biomater. 9 (2013) 6032–6040.
[36] J.J. Stankus, L. Soletti, K. Fujimoto, Y. Hong, D.A. Vorp, W.R. Wagner, Biomaterials 28 (2007) 2738–2746.
[37] G. Konig, T.N. McAllister, N. Dusserre, S.A. Garrido, C. Iyican, A. Marini, A. Fiorillo, H. Avila, W. Wystrychowski, K. Zagalski, M. Maruszewski, A.L. Jones, L. Cierpka, L.M. de la Fuente, N. L'Heureux, Biomaterials 30 (2009) 1542–1550.
[38] K. Zhang, A. Yin, C. Huang, C. Wang, X. Mo, S.S. Al-Deyab, M. El-Newehy, Polym. Degrad. Stab. 96 (2011) 2266–2275.
[39] J. Peña, T. Corrales, I. Izquierdo-Barba, A.L. Doadrio, M. Vallet-Regí, Polym. Degrad. Stab. 91 (2006) 1424–1432.
[40] I.R.C.Y. Xu, M.Y. Kotaki, S. Ramakrishna, Tissue Eng. 10 (2004) 1160–1168.
[41] C. Huang, R. Chen, Q. Ke, Y. Morsi, K. Zhang, X. Mo, Colloids Surf. B: Biointerfaces 82 (2011) 307–315.
[42] B.W. Tillman, S.K. Yazdani, S.J. Lee, R.L. Geary, A. Atala, J.J. Yoo, Biomaterials 30 (2009) 583–588.
[43] H.J.Y. Liu, Y. Li, K. Zhu, Chin. J. Polym. Sci. (Engl. Ed.) 26 (2008) 63–71.
[44] K. Kim, M. Yu, X. Zong, J. Chiu, D. Fang, Y.-S. Seo, B.S. Hsiao, B. Chu, M. Hadjiargyrou, Biomaterials 24 (2003) 4977–4985.